Inorganic Chemistry

Article

pubs.acs.org/IC

Synthesis and Electrochemical Properties of *cis*- and *trans*-$[Mo_2(O_2C\text{-}Fc)_2(DArF)_2]$ (O_2C-Fc = Ferrocenecarboxylate; DArF = *N,N′*-Diarylformamidinate)

Xu-Min Cai,[†] Teresa K. Zimmermann,[†] Alexander Pöthig,[‡] and Fritz E. Kühn*[,†,§]

[†]Molecular Catalysis, Department of Chemistry and Catalysis Research Center (CRC), Technische Universität München (TUM), Lichtenbergstrasse 4, 85747 Garching bei München, Germany

[‡]CRC, Ernst-Otto-Fischer-Straße 1, 85747 Garching bei München, Germany

Supporting Information

ABSTRACT: The reaction of *cis*-$[Mo_2(O_2C\text{-}Fc)_2(NCCH_3)_4][BF_4]_2$ (***cis*-1**) with three electronically different *N,N′*-diarylformamidinate (DArF) ligands [DArF = *N,N′*-diphenylformamidinate (DPhF), *N,N′*-di(*p*-trifluoromethylphenyl)formamidinate (DTfmpF), and *N,N′*-di(*p*-anisyl)formamidinate (DAniF)] results in products of the general composition $[Mo_2(O_2C\text{-}Fc)_2(DArF)_2]$. Even though the *trans*-$[Mo_2(O_2C\text{-}Fc)_2(DArF)_2]$ isomers were originally expected to be the sole products, the corresponding *cis*-$[Mo_2(O_2C\text{-}Fc)_2(DArF)_2]$ complexes were isolated as well via crystallization and verified unambiguously by X-ray crystallography. All novel complexes, namely, *cis*-$[Mo_2(O_2C\text{-}Fc)_2(DPhF)_2]$ (***cis*-2a**), *cis*-$[Mo_2(O_2C\text{-}Fc)_2(DTfmpF)_2]$ (***cis*-2b**), and *trans*-$[Mo_2(O_2C\text{-}Fc)_2(DAniF)_2]$ (***trans*-2c**), were studied regarding their electrochemical properties with respect to electrolyte, solvent, and ligand. The electron-donating ligand $DArF^-$ enables the oxidation of the $[Mo_2]^{4+}$ unit prior to that of Fc, while the oxidation sequence is reversed when acetonitrile or diphosphine ligands are coordinated instead of formamidinate. In the case of *trans*-$[Mo_2(O_2C\text{-}Fc)_2(DAniF)_2]$, interactions were found between the two redox-active ferrocenecarboxylate ligands, with a clear $\Delta E_{1/2}$ value originating from the peak-to-peak separation in DPV of around 100 mV with CH_2Cl_2 as solvent. Furthermore, the second oxidation of the Mo_2-handle $[Mo_2]^{5+}/[Mo_2]^{6+}$ was exclusively observed with $DAniF^-$ as the ligand. Similar absorption patterns in UV−vis spectra were found within the series **2a**−**2c**, corresponding to similar structural and electronic features of the complexes.

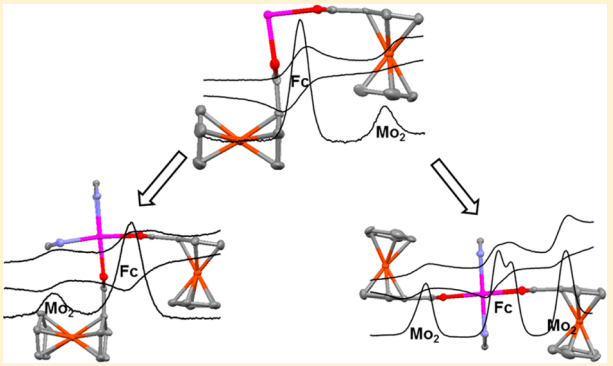

INTRODUCTION

After the first quadruply bonded dimetal complex $[Re_2Cl_8]^{2-}$ was discovered half a century ago,[1] the prosperous field of dinuclear paddle-wheel (PW) complexes possessing a quadruple bond (electron configuration of $\sigma^2\pi^4\delta^2$; e.g., Cr, Mo, and W) emerged.[2−10] Particularly for the Mo_2 systems, detailed studies focusing on both structural and electrochemical features, which vary strongly depending on equatorial ligation, have been reported.[11−23] As it is the case for its bis-substituted derived complexes, *cis*-$[Mo_2(DAniF)_2(NCCH_3)_4][BF_4]_2$ was frequently applied for synthesizing molecular cyclic structures,[8,24−27] whereas its congener *trans*-$[Mo_2(DAniF)_2(NCCH_3)_4][BF_4]_2$ might possibly be used for ladder type oligomers.[28,29] Among these above-mentioned compounds, electronic coupling between the metal centers has often been reported. Therefore, Mo_2 moieties possessing cis and trans configuration have recently attracted some attention due to the possibility for both redox-active cyclic and ladder type structures. Our interest involves the controllable equatorial ligation to both cis and trans redox-active entities based on the trans effect order according to increasing ligand lability: $DArF^- > R{-}CO_2^- > CH_3CN$.[30] In the literature, the ligand basicity (which correlates to ligand lability) order was reported as proportional to the trans effect;[30] hence, both structural motifs and the electrochemical behaviors of Mo_2 system can be interpreted according to this basicity rule.

Structural Motifs. Carboxylate ligands $R{-}CO_2^-$ can readily substitute the weakly coordinating CH_3CN of the precursor compound $[Mo_2(NCCH_3)_{10}][BF_4]_4$, typically yielding *cis*-$[Mo_2(O_2C\text{-}R)_2(NCCH_3)_4][BF_4]_2$.[3,31,32] In contrast, both *cis*- and *trans*-$[Mo_2(DArF)_2(NCCH_3)_4][BF_4]_2$ were synthesized directly and indirectly from $[Mo_2(DArF)_4]$.[30,33] All these *bis*-substituted reactants can be further used as precursors for cis and trans conformers, exemplarily shown in Scheme 1. On the basis of previous assumptions, *cis*-$[Mo_2(DAniF)_2(NCCH_3)_4][BF_4]_2$ should react to *cis*-$[Mo_2(DAniF)_2(O_2C{-}CH_3)_2]$ only (reaction a), while, *cis*-$[Mo_2(O_2C{-}CH_3)_2(NCCH_3)_4][BF_4]_2$ should be converted exclusively to *trans*-$[Mo_2(DAniF)_2(O_2C{-}CH_3)_2]$ (reaction b) due to the stronger trans effect of $DAniF^-$ over $CH_3{-}CO_2^-$.[30] Unfortunately, reaction b have not yet been

Received: April 29, 2015
Published: June 18, 2015

DOI: 10.1021/acs.inorgchem.5b00964
Inorg. Chem. 2015, 54, 6631−6640

Scheme 1. Reaction Conditions for Selected Processes[a]

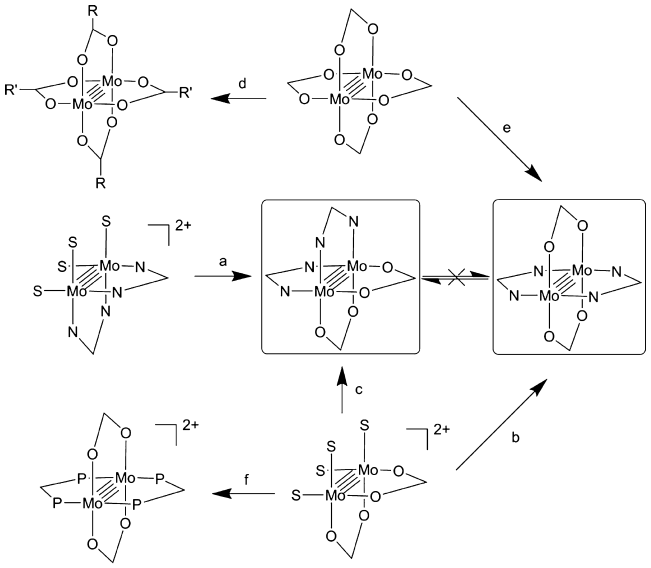

[a]S = CH_3CN.

investigated in detail. Previous efforts to synthesize both cis and trans products from *cis*-$[Mo_2(O_2C{-}CH_3)_2(NCCH_3)_4][BF_4]_2$ were reported by Dunbar et al. (reactions b and c) based on axial appendage of the equatorial ligand.[34] When $[Mo_2(O_2C\text{-}R)_4]$ is applied as precursor, the trans positions can be substituted by either $R'{-}CO_2^-$ or $DArF^-$ (reactions d and e).[11,13,14,28,30,35−37] The fact that *trans*-$[Mo_2(O_2C\text{-}R)_2(DPPX)_2][BF_4]_2$ (DPPX = diphosphine, e.g., DPPE for 1,2-bis(diphenylphosphino)ethane; reaction f) can be obtained according to Scheme 1 is most likely ascribed to the steric effect of DPPX.[15,31,32]

Redox Behavior. For $[Mo_2(DArF)_4]$, oxidation of $[Mo_2]^{4+}$ can be unambiguously assigned to the removal of an electron from the Mo−Mo δ bonding orbital,[38] with the $[Mo_2]^{4+}/[Mo_2]^{5+}$ oxidation potential in the range of −0.2 to 0.4 V (vs F_c/F_c^+; same below).[39] When the more basic ligand guanidinate was applied in $[Mo_2(hpp)_4]$ (hpp = the anion of 1,3,4,6,7,8-hexahydro-2*H*-pyrimido[1,2-*a*]pyrimidine), the $[Mo_2]^{4+}$ unit is oxidized at a very low potential ($E_{1/2}$ $[Mo_2]^{4+}/[Mo_2]^{5+}$ at −1.7 V), so that it can even be applied as a reducing agent.[40] However, in the case of $[Mo_2(O_2C\text{-}R)_4]$, oxidation is more difficult compared to $[Mo_2(DArF)_4]$.[41,42] Interestingly, the $[Mo_2]^{4+}$ unit in $[Mo_2(NCCH_3)_{10}][BF_4]_4$[15] exhibits a very positive oxidation potential of ca. 1.7 V, compared to that in $[Mo_2(hpp)_4]$ of −1.7 V, although both of them possess an identical electron configuration of $\sigma^2\pi^4\delta^2$. Similarly, $[Mo_2]^{4+}/[Mo_2]^{5+}$ oxidation was observed at ca. 1.3 V in the case of *trans*-$[Mo_2(O_2C\text{-}Fc)_2(DPPX)_2][BF_4]_2$.[15] Considering the results mentioned above, it can be concluded that the oxidation potential of $[Mo_2]^{4+}/[Mo_2]^{5+}$ is very sensitive to the nature of the equatorial ligand. It is likely that the oxidation potential $E_{1/2}([Mo_2]^{4+}/[Mo_2]^{5+})$ can be correlated to ligand basicity, which decreases in the order hpp > $DArF^-$ > $R{-}CO_2^-$ > DPPX > CH_3CN. Recently, a number of detailed studies concerning the δ bond have been published, attempting to clarify the correlation between the δ bond energy and the relative ligand orbitals.[35,43−46] Although no general molecular orbital diagram can be applied for the Mo_2 system, a strong interaction between the δ bond energy and the nature of the equatorial ligands can be assumed.[38,39]

In this work the first example of a one-pot reaction of the cis precursor ***cis*-1** to both *cis*- and *trans*-$[Mo_2(O_2C\text{-}Fc)_2(DArF)_2]$ isomers (reactions *b* and *c*) is presented. This discovery contrasting previous assumptions concerning the synthesis of cis- and trans-isomers might be ascribed to the similar basicity of $DArF^-$ and $Fc{-}CO_2^-$, both of which are more basic than acetate.[30,47,48] A reaction mechanism regarding the relevant reaction intermediates is proposed because no interconversion of the cis and trans product could be observed (see Scheme 1). In addition, electrochemical investigation of the complex series revealed similar $[Mo_2]^{4+}/[Mo_2]^{5+}$ oxidation potentials in all products to that obtained for $[Mo_2(DArF)_4]$, illustrating the apparently similar basicity of $DArF^-$ and $Fc{-}CO_2^-$. Consequently, ligand basicity appears to decrease in the following order: hpp > $DArF^-$ (∼ $Fc{-}CO_2^-$) > $R{-}CO_2^-$ (R = alkyl) > DPPX > CH_3CN.

Scheme 2. Synthesis of Compounds 2a−2c[a]

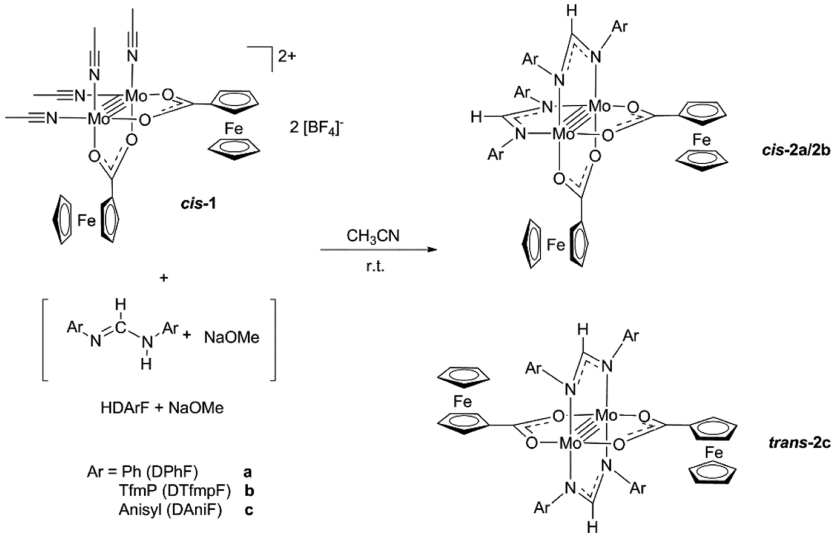

[a]A mixture of cis and trans isomers was obtained in each crude product.

DOI: 10.1021/acs.inorgchem.5b00964
Inorg. Chem. 2015, 54, 6631−6640

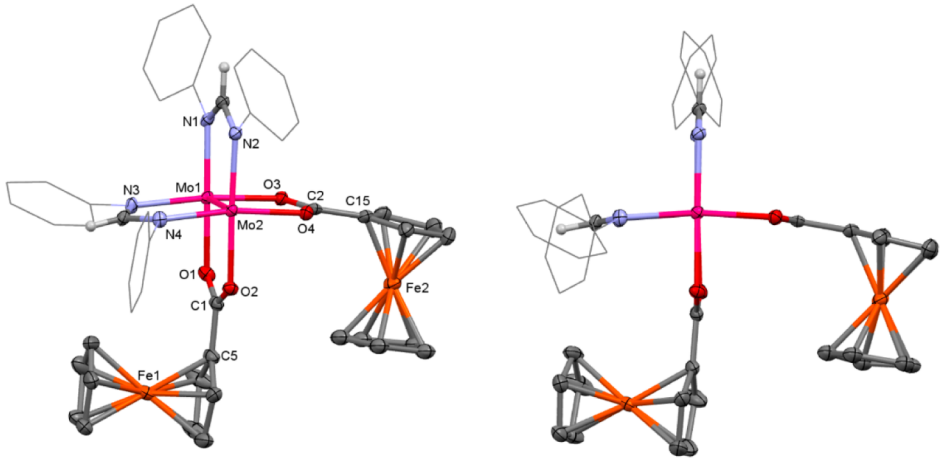

Figure 1. Perspective drawing of molecular structure of ***cis*-2a** (left; thermal ellipsoids are shown at a probability level of 50%) and side view (right). Aryl groups are shown as wireframes, and hydrogen atoms (except for those on the $DPhF^-$ bridges) and non-coordinating solvent molecules (CH_2Cl_2) are omitted for clarity.

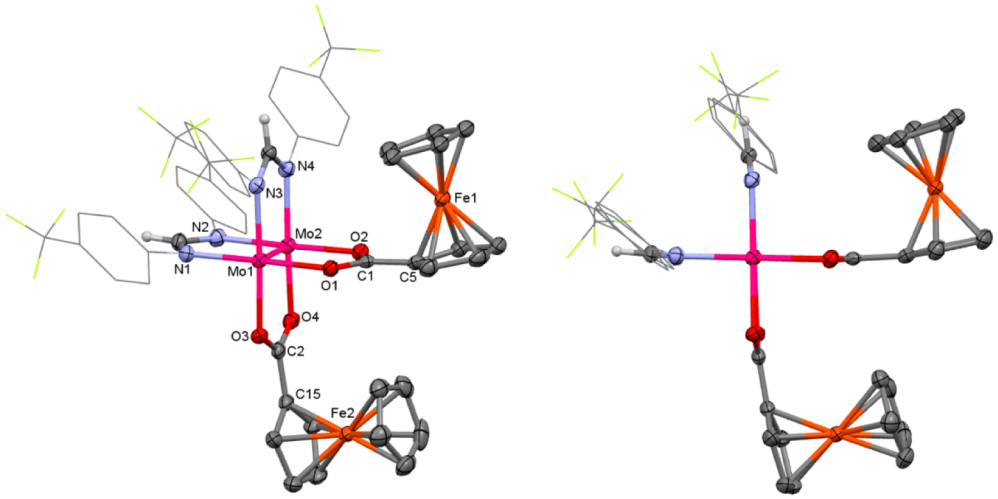

Figure 2. Perspective drawing of molecular structure of ***cis*-2b** (left; thermal ellipsoids are shown at a probability level of 50%) and side view (right). Aryl groups are shown as wireframes, and hydrogen atoms (except for those on the $DTfmpF^-$ bridges) are omitted for clarity.

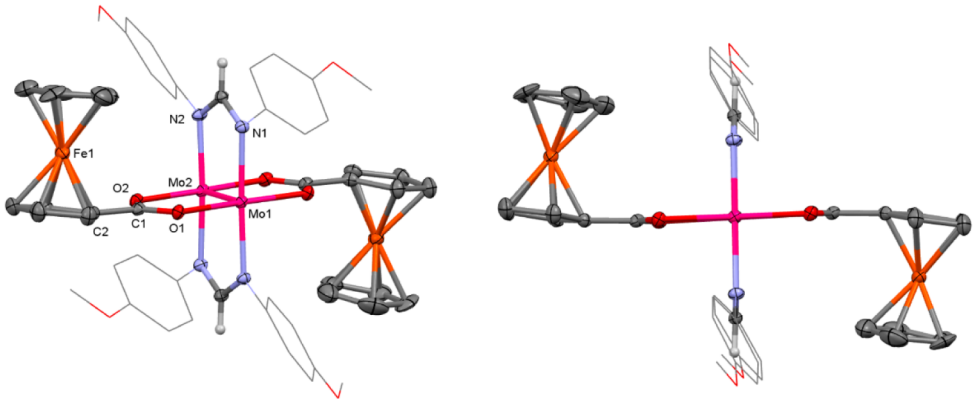

Figure 3. Perspective drawing of molecular structure of ***trans*-2c** (left; thermal ellipsoids are shown at a probability level of 50%) and side view (right). Aryl groups are shown as wireframes, and hydrogen atoms (except for those on the $DAniF^-$ bridges) and non-coordinating solvent molecules (CH_2Cl_2) are omitted for clarity. Symmetry operation for equivalent atoms: $1 - x, 1 - y, z$.

RESULTS AND DISCUSSION

Syntheses. All $DArF^-$ ligands were prepared independently via dissolving sodium methoxide and the corresponding formamidine (HDArF) in CH_3CN, where the white solid turns into a yellow solution immediately. The yellow solution was stirred for 15 min before adding it to an acetonitrile solution of cis-1. The reaction of dark red **cis-1** and a corresponding amount of $DArF^-$ at room temperature rapidly yields an orange

DOI: 10.1021/acs.inorgchem.5b00964
Inorg. Chem. 2015, 54, 6631−6640

Table 1. Crystallographic Data for Compounds 2a−2c

	cis-2a	*cis*-2b	*trans*-2c
formula	$C_{50}H_{44}N_4Cl_4Fe_2Mo_2O_4$	$C_{52}H_{36}N_4F_{12}Fe_2Mo_2O_4$	$C_{54}H_{52}Cl_4Fe_2Mo_2N_4O_8$
M_r	1210.27	1312.43	1330.42
crystal habit	clear intense orange fragment	clear intense orange fragment	clear intense orange plate
crystal system	triclinic	monoclinic	orthorhombic
space group	$P\bar{1}$	$P2_1/n$	$Fdd2$
a [Å]	10.1219(14)	14.1318(9)	40.3405(11)
b [Å]	11.3899(16)	20.6839(13)	11.5252(3)
c [Å]	21.056(3)	18.6472(12)	22.8422(6)
α [°]	97.160(7)	90	90
β [°]	90.056(7)	92.903(3)	90
γ [°]	102.386(7)	90	90
V [Å^3]	2351.5(6)	5443.6(6)	10620.1(5)
Z	2	4	8
ρ_c [g cm^{-3}]	1.709	1.601	1.664
$F(000)$	1216	2608	5376
T [K]	123	123	123
μ [mm^{-1}]	1.404	1.060	1.257
data/restraints/parameters	10784/344/697	9946/301/815	10392/201/383
GoF (F^2)	1.035	1.048	1.049
R_1[a], wR_2[b] ($I > 2\sigma(I)$)	0.0404, 0.1148	0.0393, 0.1021	0.0358, 0.0804
R_1, wR_2 (all data)	0.0501, 0.1228	0.0552, 0.1099	0.0468, 0.0852
R_{int}	0.0669	0.0890	0.0382

[a] $R_1 = \Sigma(||F_0| - |F_c||)/\Sigma|F_0|$. [b] $wR_2 = \{\Sigma[w(F_0^2 - F_c^2)^2]/\Sigma[w(F_0^2)^2]\}^{1/2}$.

precipitate, which exhibits a very small but distinct difference in the chemical shift of the −NCHN− fragment in ^{1}H NMR spectra (Figures S4−S6 in the Supporting Information, SI), illustrating the coexistence of both cis and trans isomers in each reaction, with an integral ratio of the major to the minor isomer of around four. The cis and trans isomers could be identified by comparison with the isolated pure isomers (vide infra). In a previous report by Cotton et al., *cis*- and *trans*-$[Mo_2(O_2C{-}CH_3)_2(DAniF)_2]$ (obtained via different synthetic strategies; see introduction) were described to exhibit a similarly small ^{1}H NMR shift variation of 0.04 ppm.[30] In our work, bright orange compounds ***cis*-2a**, ***cis*-2b**, and ***trans*-2c** were exclusively isolated as the main isomers via crystallization in 25%, 20%, and 25% crystalline yield, respectively, as shown in Scheme 2. In order to selectively obtain one pure isomer, reactions at both low temperature (−20 °C) and high temperature (60 °C) were carried out. However, a similar isomer ratio was found at both temperatures. Thus, room temperature was finally applied for all reactions.

Crystal Structure Discussion. Single crystals suitable for X-ray diffraction experiments could be obtained for all products. Crystallization of all products from CH_2Cl_2 solution layered with *n*-pentane and diethyl ether revealed the retention of cis disposition in ***cis*-2a** and ***cis*-2b** (Figures 1 and 2) and ligand transformation arrangement in ***trans*-2c** (Figure 3). The crystallographic data are summarized in Table 1, while selected bond lengths and angles are listed in Table 2.

All products crystallize in different space groups, varying from triclinic, monoclinic, to orthorhombic with Z values of 2, 4, and 8 for ***cis*-2a**, ***cis*-2b**, and ***trans*-2c**, respectively, which reflects the sensitivity of the packing pattern (Figures S1−S3) toward the nature of the ligands. An essentially eclipsed coordination geometry for the Mo_2 core was observed in all side views, where the averaged torsion angles N−Mo1−Mo2−O amount to 175.66 and 179.33° for ***cis*-2a** and ***cis*-2b**, and N−Mo1−Mo2−N and O−Mo1−Mo2−O are 179.76 and 179.14° for ***trans*-2c**, respectively. Although the structural motif of ***cis*-2a** and ***cis*-2b** is quite similar, the aryl groups are arranged in a rather different manner: the aryl rings appear to be nearly parallel in ***cis*-2b**, while they are relatively disordered in ***cis*-2a.** This might be attributed to packing effects in the solid state. Further, the torsion angle

Table 2. Selected Bond Lengths (Å) and Angles (deg) for Compounds 2a−2c

	cis-2a	*cis*-2b	*trans*-2c
Mo1−Mo2	2.0852(4)	2.0812(5)	2.0791(4)
Mo1−O1	2.120(2)	2.120(2)	2.111(2)
Mo1−O3	2.139(2)	2.095(2)	
Mo2−O2	2.136(2)	2.107(2)	2.108(2)
Mo2−O4	2.114(2)	2.112(2)	
Mo1−N1	2.124(2)	2.124(3)	2.150(3)
Mo1−N3	2.135(2)	2.125(3)	
Mo2−N2	2.138(2)	2.127(3)	2.132(3)
Mo2−N4	2.106(2)	2.131(3)	
C1−O1	1.269(4)	1.271(4)	1.274(4)
C1−O2	1.273(3)	1.283(4)	1.278(4)
C2−O3	1.268(3)	1.276(4)	
C2−O4	1.273(3)	1.276(4)	
C1−C2			1.460(4)
C1−C5	1.462(4)	1.464(5)	
C2−C15	1.468(4)	1.453(5)	
Fe···Fe′	7.4227(9)	7.2734(3)	10.7750(2)
$C_\omega{\cdots}C_\omega{}'$[a]	5.6748(8)	5.6653(3)	8.3681(2)
Fe1−C2−C2−Fe1			−171.22
N1−Mo1−Mo2−O2	−179.91	179.76	
N2−Mo2−Mo1−O1	177.27	179.63	
N3−Mo1−Mo2−O4	172.31	178.64	
N4−Mo2−Mo1−O3	−173.15	179.30	
N1−Mo1−Mo2−N2			−179.76
O1−Mo1−Mo2−O2			179.14

[a] C_ω and $C_\omega{}'$ denote Cp carbon atoms covalently bonded to $-CO_2$ unit.

DOI: 10.1021/acs.inorgchem.5b00964
Inorg. Chem. 2015, 54, 6631−6640

Fe1−C2−C2A−Fe1A of −171.22° for ***trans*-2c** illustrates the linear *trans*-arrangement of the Fc−CO_2^- moieties.

The Mo−Mo bond lengths of **2a−2c** are approximately 2.08 Å and thus lie in the typical range for tetra-chelating Mo_2 complexes with $DArF^-$ as ligand,[2,39] and are around 0.05 Å shorter than that of 2.1315(7) Å in the bis-chelating precursor ***cis*-1**.[3] The remaining bond lengths of ***trans*-2c** are very similar to those of ***cis*-2a** and ***cis*-2b**, although with a different ligand arrangement. Both the edge−edge distances between two Fc centers $C_\omega\cdots C_\omega'$ (C_ω and C_ω' denote the Cp carbon atoms covalently bonded to the $-CO_2$ unit) of 5.67 and 5.67 Å and the Fe···Fe′ distances of 7.42 and 7.27 Å in ***cis*-2a** and ***cis*-2b** are similar to those of 5.66 and 7.25 Å in ***cis*-1**. Because of the different coordination modes, the corresponding distances in ***trans*-2c** (8.37 and 10.78 Å) are much longer and are further discussed as part of the electrochemical investigations.

NMR Spectroscopy. Complexes **2a−2c** are diamagnetic and therefore suitable for NMR spectroscopic investigations in CD_2Cl_2 (Figures S7−S14 in the SI). The ^{13}C NMR spectrum of ***cis*-2b** is relatively complex because of the coupling of the phenyl carbons to the fluorine atoms in the $-CF_3$, resulting in three quadruplet resonances. The $^3J_{CF}$, $^2J_{CF}$, and $^1J_{CF}$ coupling constants are found to be 3.70, 32.4, and 270 Hz, respectively. 2D NMR spectroscopy was employed for detailed analysis (Figures 4 and S15−S17). For the DAniF fragment in ***trans*-2c**,

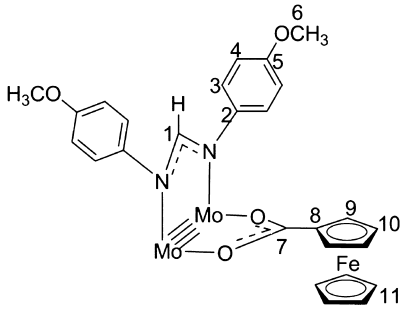

Figure 4. Labeled fragment of ***trans*-2c** for interpretation of NMR spectra.

H_1 can be assigned to the peak at 8.60 ppm, which corresponds to C_1 at 156.6 ppm according to HSQC. Likewise, the signal of H_6 (3.73 ppm) corresponds to the signal at 55.94 ppm of C_6. Further, C_2 and C_5 correspond to the signals at 143.1 and 156.9 ppm, respectively, because direct correlations to protons in HSQC are absent, while indirect correlations of C_2 to H_1 and C_5 to H_6 can be observed in HMBC. With regard to the remaining two sets of protons/carbons (H_3/C_3 and H_4/C_4) on the phenyl rings, both HSQC and HMBC are needed for interpretation. The signals at 6.69/114.8 ppm can be attributed to signals of H_3/C_3 (indirect correlation of H_3 to C_2 in HMBC), while H_4/C_4 correspond to the signals found at 6.73/123.6 ppm (indirect correlation of H_4 to C_5 in HMBC). Regarding the Fc fragment, the protons on the unsubstituted Cp ring (H_{11}) can be assigned to the signal at 4.10 ppm, which corresponds to C_{11} at 70.71 ppm according to HSQC. Further, the resonance of C_8 is assigned to the signal at 74.68 ppm because of the absence of direct proton correlation. Both HSQC and HMBC are again applied for the interpretation of the remaining two sets of protons/carbons, H_9/C_9 and H_{10}/C_{10}, with the former set assigned to the signals at 4.39/71.56 ppm, and the latter to those at 4.98/70.82 ppm (indirect correlation of H_9 to C_8 in HMBC). A fluxional behavior of the two Fc units of ***cis*-2a/2b** in solution is assumed because only one set of proton signals can be observed, while the Fc arrangement found in the X-ray crystal structures could result in multiple resonances.[15] Although electronically different $DArF^-$ ligands are coordinated, the signals of the Cp ring protons are rather close, indicating minor electronic impact on the Fc units. Both the electron-donating capability of $DArF^-$ and its influence on the Fc unit will be further discussed as part of electrochemical investigations.

UV−vis Spectroscopy. The UV−vis absorption spectra of compounds ***cis*-1** and **2a−2c** in CH_2Cl_2 are shown in Figure 5.

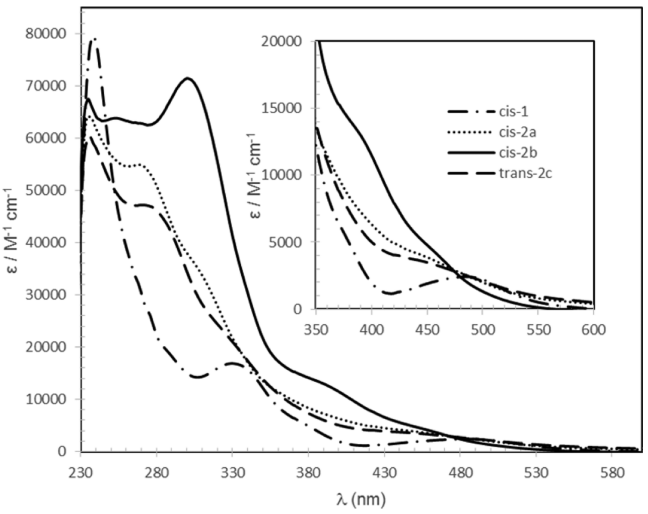

Figure 5. UV−vis spectra of compounds **1** and **2a−2c** in CH_2Cl_2. No absorption bands are observed beyond 600 nm.

In the literature, the low-energy absorption in the region of 400−600 nm are assigned to a $\delta \rightarrow \delta^*$ transition in Mo_2 systems.[2,32,33] All products **2a−2c** reported in this paper show weak shoulder absorptions in this region, which may be due to this orbital transition. The low-energy absorptions of **2a−2c** at 450, 460, and 450 nm, respectively, are blue-shifted around 35 nm compared to that in ***cis*-1** (490 nm), which corresponds well to the observation in previous studies[49] that the higher the number of chelating ligands, the higher the transition energy ΔE ($\delta \rightarrow \delta^*$). The similar ΔE values observed for all products are in agreement with a report on $[Mo_2(DArF)_4]$ complexes, illustrating the very small influence over $\delta \rightarrow \delta^*$ transition energy from remote substituents.[39] The high-energy absorptions in the UV region may be ascribed to the ligand-based charge transfer (peaks at around 240 nm) and ligand to metal charge transfer (the remaining peaks and shoulders).[38,39] Additionally, a rather strong solvent dependence was observed for precursor ***cis*-1**, with an absorption band at 490 nm in CH_2Cl_2 and 564 nm in CH_3CN.[14]

Electrochemical Investigations. In order to shed light on the completely different electrochemical behavior of Mo_2 complexes bearing formamidinate ligands as described here as well as in Cotton's publications[24,27,50,51] and diphosphines as mentioned in a previous study,[15] both cyclic voltammetry (CV) and differential pulse voltammetry (DPV) were performed at variable testing conditions: T1, CH_2Cl_2 and $[n\text{-}Bu_4N][PF_6]$; T2, CH_2Cl_2, and $[n\text{-}Bu_4N][BF_4]$; and T3, CH_2Cl_2/CH_3CN (1/1) and $[n\text{-}Bu_4N][BF_4]$. All DPVs of the products are illustrated in Figure 6, along with CVs in Figures S18−S22 in the Supporting Information. Relevant data obtained from all figures are collected

DOI: 10.1021/acs.inorgchem.5b00964
Inorg. Chem. 2015, 54, 6631−6640

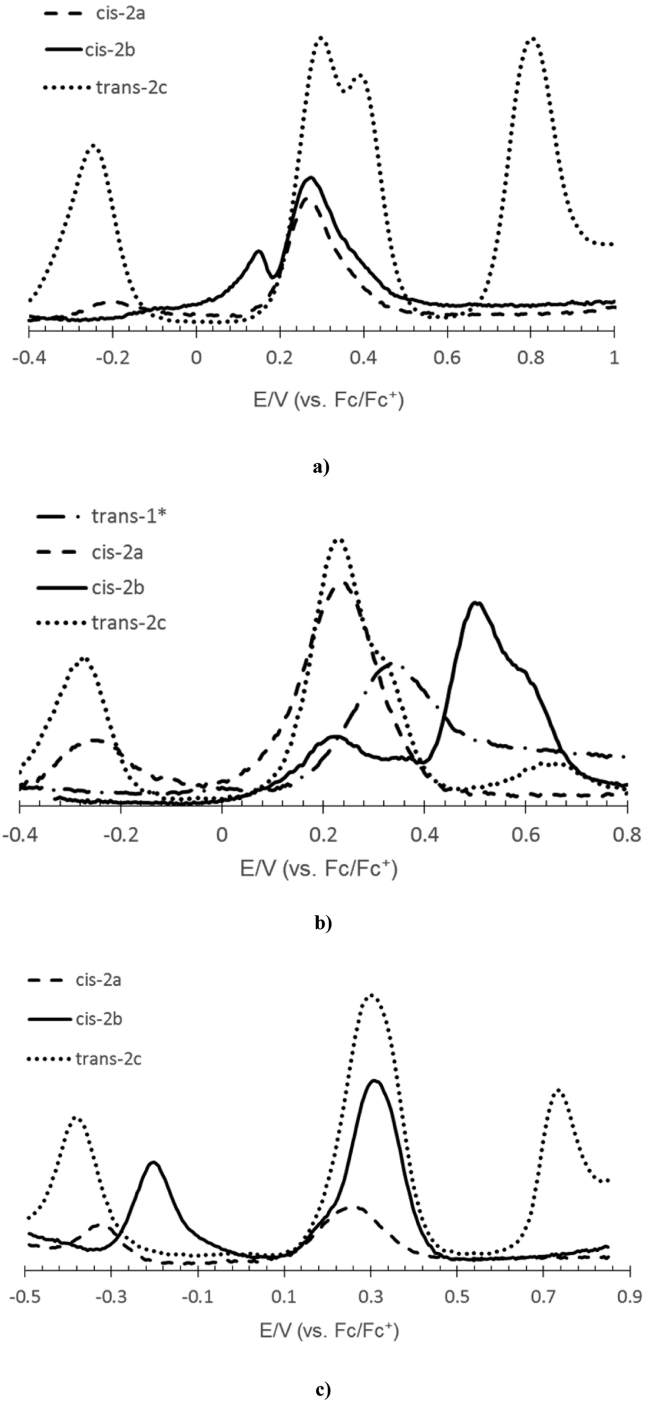

Figure 6. DPVs of Mo_2 complexes recorded in (a) a 0.10 M CH_2Cl_2 solution of electrolyte [*n*-Bu_4N][PF_6] (top; T1); (b) a 0.10 M CH_2Cl_2 solution of electrolyte [*n*-Bu_4N][BF_4] (center; T2); and (c) a 0.10 M solvent mixture of CH_2Cl_2/CH_3CN (1/1) solution of electrolyte [*n*-Bu_4N][BF_4] (bottom; T3). All the potential values are referenced to F_c/F_c^+.

in Table 3, and all of the potential values are referenced to Fc/Fc^+.

The previously reported complexes ***cis*-1** and *trans*-[Mo_2(O_2C-Fc)$_2$(DPPE)$_2$][BF_4]$_2$ (***trans*-1***)[15] exhibit oxidation potentials of $[Mo_2]^{4+}/[Mo_2]^{5+}$ at roughly 0.82 and 1.26 V, respectively (Figures S21 and S22), being quite different from the values observed for Cotton's systems (ca. −0.20 to 0.13 V vs Fc/Fc^+).[27,50] CV and DPV investigations of all Mo_2 complexes under the three examination conditions T1, T2, and T3 were intended to give a detailed interpretation with regard to the anionic ($DArF^-$) and neutral (DPPE) ligand. From Figure 6, it is evident that a similar redox sequence to Cotton's system was obtained for all products, with $[Mo_2]^{4+}$ preferentially oxidized before Fc. Therefore, the assignment of the subsequent redox processes can be carried out as follows (Scheme 3): (i) E^1 represents the first Mo_2-based oxidation process $E_{1/2}([Mo_2]^{4+}/[Mo_2]^{5+})$. (ii) The second oxidation E^2 is ascribed to the first Fc-based redox step $E_{1/2}(F_c/F_c^+)$ at the ferrocenecarboxylate ligand, closely followed by the third process E^3 centered on the further oxidation of Fc unit $E_{1/2}(F_c^+/F_c^{2+})$. (iii) Interestingly, the fourth oxidation E^4 can be only found in ***trans*-2c** and is ascribed to the process of $E_{1/2}([Mo_2]^{5+}/[Mo_2]^{6+})$.

E^1 exhibits a higher degree of reversibility in ***trans*-2c** compared to ***cis*-1** and ***trans*-1***, seen in all CV spectra. No obvious difference of redox processes between both electrolytes is observed (T1 and T2; Figure 6a,b), while they do vary in different solvents (T2 and T3; Figure 6b,c). Electrolyte [*n*-Bu_4N][BF_4] was applied to account for the anion in complex ***trans*-1***.[15] As shown in Figures 6b and S19, ***trans*-1*** only undergoes Fc-based oxidation (around 0.35 V) when CH_2Cl_2 is used as the sole solvent. However, oxidation of the $[Mo_2]^{4+}$ unit at about 1.26 V (Figures S21 and S22) is revealed when the solvent mixture CH_2Cl_2/CH_3CN is applied (close to that of 1.39 V in sole solvent CH_3CN[15]). This is due to the axial coordination of the solvent to the $[Mo_2]^{4+}$ unit. Such a solvent stabilization effect of the $[Mo_2]^{4+}$ unit could also be observed when comparing products **2a−2c** in Figure 6b,c. All $[Mo_2]^{4+}/[Mo_2]^{5+}$ oxidation values (E^1) of **2a−2c** in T3 are negatively shifted compared to $E^1([Mo_2]^{4+}/[Mo_2]^{5+})$ in T2, especially in the case of ***cis*-2b** (from 0.23 to −0.19 V).

Apart from the influence of electrolyte and solvent, the electron-donating effect of the equatorial $DArF^-$ ligand is considered to be responsible for the oxidation overturn of the $[Mo_2]^{4+}/[Mo_2]^{5+}$ and Fc units when comparing diphosphine- and formamidinate-coordinating systems (***trans*-1*** and **2a−2c**). As observed in Figures 6c and S22, E^1 in products **2a−2c** (−0.31, −0.19, and −0.36 V, respectively) are shifted to lower potentials by about 1.50 V compared to E^1 in ***trans*-1*** (1.26 V), apparently due to the strong electron-donating capability of $DArF^-$. However, such an effect would be expected to be greatly attenuated on the Fc units over the large distance, which is in accord with similar Fc-based oxidation potentials of around 0.30 V (Table 3). More interestingly, no matter what the testing conditions, oxidation of $[Mo_2]^{5+}/[Mo_2]^{6+}$ (E^4) is observed exclusively at about 0.60−0.80 V in ***trans*-2c**, most likely due to the strong electron-donating character of the methoxyl substituent. So far, chemical oxidation of $[Mo_2]^{5+}$ to $[Mo_2]^{6+}$ was only reported in the very basic guanidinate-coordinating complexes such as $[Mo_2(hpp)_4]$, where $E_{1/2}([Mo_2]^{5+}/[Mo_2]^{6+})$ = −0.97 V.[40,52] Except for this particular case, only the first oxidation of $[Mo_2]^{4+}$ to $[Mo_2]^{5+}$ in the easily oxidized complexes $[Mo_2(DArF)_4]$ was mentioned at potentials from −0.30 to 0.25 V.[39] It was concluded that the $[Mo_2]^{4+}$ moiety is very sensitive to small variations at the $DArF^-$ substituents,[39] which corresponds well with our observations with E^1 in ***cis*-2b** (−0.19 V) of 120 and 170 mV higher than E^1 in ***cis*-2a** (−0.31 V) and ***trans*-2c** (−0.36 V), respectively (in T3). This oxidation potential difference ($E^1_{cis\text{-}2b} - E^1_{cis\text{-}2a/trans\text{-}2c}$) in T3 is smaller than that in cases of T1 and T2 (from 350 mV to 510 mV) due to the axial electron-donating CH_3CN in T3, which therefore counteracts the strong electron-withdrawing effect of $-CF_3$ substituent in ***cis*-2b**. The

DOI: 10.1021/acs.inorgchem.5b00964
Inorg. Chem. 2015, 54, 6631−6640

Table 3. Electrochemical Data (in V) for All Compounds (vs. F_c/F_c^+)

compd	experimental condition	E^1	E^2	E^3	$E_{1/2}$ (F_c/F_c^{2+})	$\Delta E_{1/2}$[a] (mV)	E^4
***cis*-1**	T1[b]						
	T2[c]						
	T3[d]	0.82			0.36		
trans-**1***	T1						
	T2				0.35		
	T3	1.26			0.38		
***cis*-2a**	T1	−0.20			0.28		
	T2	−0.25			0.25		
	T3	−0.31			0.27		
***cis*-2b**	T1	0.15	0.28	0.38		100	
	T2	0.23	0.51	0.61		100	
	T3	−0.19			0.32		
***trans*-2c**	T1	−0.24	0.30	0.40		100	0.81
	T2	−0.28	0.24	0.34		100	0.66
	T3	−0.36			0.31		0.74

[a]Calculated from the difference between $E_{1/2}(F_c^+/F_c^{2+})$ and $E_{1/2}(F_c/F_c^+)$ obtained from DPV. [b]T1 represents experimental conditions in CH_2Cl_2 and [*n*-Bu_4N][PF_6]. [c]T2 represents experimental conditions in CH_2Cl_2 and [*n*-Bu_4N][BF_4]. [d]T3 represents experimental conditions in CH_2Cl_2/CH_3CN (1/1) and [*n*-Bu_4N][BF_4].

Scheme 3. Assignment of the Step-by-Step Redox Processes

$$[Fe^{II}Mo_2^{II,II}Fe^{II}]^0 \underset{E^1}{\overset{-e^-}{\rightleftharpoons}} [Fe^{II}Mo_2^{II,III}Fe^{II}]^+ \underset{E^2}{\overset{-e^-}{\rightleftharpoons}} [Fe^{III}Mo_2^{II,III}Fe^{II}]^{2+} \underset{E^3}{\overset{-e^-}{\rightleftharpoons}} [Fe^{III}Mo_2^{II,III}Fe^{III}]^{3+} \underset{E^4}{\overset{-e^-}{\rightleftharpoons}} [Fe^{III}Mo_2^{III,III}Fe^{III}]^{4+}$$

fact that ***cis*-2a** and ***trans*-2c** are a lot more sensitive to air and moisture than ***cis*-2b** and ***trans*-1*** is in good agreement with the ready oxidation of E^1 in all compounds.

In addition, electronic coupling is observed as expected in both CV and DPV, with a clear split of $\Delta E_{1/2}$ (around 100 mV) in ***trans*-2c** between the *trans*-positioned Fc units. The $\Delta E_{1/2}$ value of ***cis*-2a** could not be observed directly, as in precursor ***cis*-1** and *cis*-[Ru_2(DmAniF)$_2$(O_2C-Fc)$_2$Cl] (DmAniF = *N*,*N*′-di(3-methoxyphenyl)formamidinate).[48] Interestingly, the $\Delta E_{1/2}$ value of ca. 100 mV in ***cis*-2b** is found nonetheless, similar to that in *cis*-[Ru_2(D(3,5-Cl_2Ph)F)$_2$(O_2C-Fc)$_2$Cl] (D(3,5-Cl_2Ph)F = *N*,*N*′-di(3,5-dichlorophenyl)formamidinate).[47] Compared to the above-mentioned cis examples with regard to the $\Delta E_{1/2}$ value, it can be assumed that the electron-withdrawing substituents on DArF$^-$ in compounds ***cis*-2b** and *cis*-[Ru_2(D(3,5-Cl_2Ph)F)$_2$-(O_2C-Fc)$_2$Cl] can visualize $\Delta E_{1/2}$ values. The reason why the $\Delta E_{1/2}$ value in T3 is not as obvious as in T1 and T2 is possibly because the electronic interaction between electron-donating acetonitrile (most likely of π bond) and the electron deficient δ bond of $[Mo_2]^{5+}$ (configuration of $\sigma^2\pi^4\delta^1$) could deteriorate the electron delocalization over the Fc-Mo_2-Fc moiety. The $\Delta E_{1/2}$ value of 100 mV could lead to the thermodynamic comproportionation constant K_c of 49, according to the equation $K_c = e^{\Delta E_{1/2}/25.69}$.[53] It is important to bear in mind that K_c is only a thermodynamic equilibrium constant that represents the stability of the mixed-valence intermediate derived from its neutral and doubly oxidized form, other than a direct measure of electronic communication. It can only be deemed as strong communication when $K_c > 10^6$ is available.[54]

Synthesis and Its Impact on Isomerization. A modified synthetic pathway compared to the literature[30] is proposed in Scheme 4. It was concluded in the literature that a cis precursor yields only the trans isomer based on the stronger trans effect of DArF$^-$ over carboxylate ($CH_3-CO_2^-$ in the mentioned publication). The reason why both isomers could be obtained here is, to some extent, ascribed to the stronger electron-donating impact of Fc$-CO_2^-$ over $CH_3-CO_2^-$, which weakens the trans effect of DArF$^-$. Given the similar basicity of Fc$-CO_2^-$ and DArF$^-$, similar crystallographic and electrochemical data for the products reported here (vide supra) and for published complexes $[Mo_2(DArF)_4]$[39] are observed. The trans effect exerted by these ligands appears to be proportional to their basicity, decreasing in the order DArF$^-$ (~Fc$-CO_2^-$) > R$-CO_2^-$ (R = alkyl group) > CH_3CN. Drawn in Scheme 4 is a proposed pathway for both the geometry retention (top) and transformation (bottom) via ligand migration. The intermediate cation *cis*-[Mo_2(O_2C-Fc)$_2$(DArF)($NCCH_3$)$_2$]$^+$ (up center) has not been isolated but appears to be the logical intermediate in the stepwise addition of one DArF$^-$ to the precursor. If a second kinetically controlled stepwise addition to this intermediate is achieved, the cis isomer would be the only product (top, right). When using the pure isomer for time-dependent ^{1}H NMR measurement, no interconversion between the cis and trans

Scheme 4. Proposed Mechanism for Isomerization via Intermediate Transformation[a]

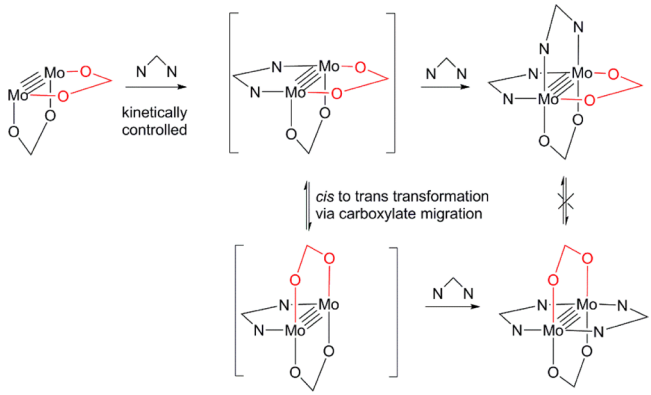

[a]Equatorial CH_3CN ligands are not shown due to the fast scrambling with solvent CH_3CN.

DOI: 10.1021/acs.inorgchem.5b00964
Inorg. Chem. 2015, 54, 6631−6640

geometries is observed, indicating that both the cis and the trans isomers are stable as synthesized. Therefore, the isomerization can only be achieved through an intermediate transformation via carboxylate migration to the position opposite to the other carboxylate (highlighted in red). This is because the remaining labile equatorial ligands CH_3CN (not shown in Scheme 4) are rapidly scrambling with the solvent CH_3CN, thus providing for the vacant position for the ligand rearrangement. The observation of both cis and trans isomers in the raw precipitate indicates the existence of an equilibrium between the two unobtainable intermediates. The cis to trans transformation mechanism was previously reported by Dunbar as acetate migration from the cleavage of one equatorial Mo−O bond to form a new axial Mo−O bond.[34] Compared to the mechanism proposed here, the Mo−O cleavage and rebonding appear to be more energy-consuming when the relatively larger ligand Fc−CO_2^- is applied rather than CH_3−CO_2^-.

CONCLUSIONS

Three novel cis and trans Mo_2 paddlewheel complexes (**2a**−**2c**) of the general composition $[Mo_2(O_2C\text{-}Fc)_2(DArF)_2]$ bearing ferrocenecarboxylate ligands have been synthesized via a one-pot reaction from the cis precursor (***cis*-1**). A mixture of both isomers has been observed in the crude product of all reaction mixtures, while the configuration of the preferentially crystallized product could be identified unambiguously via X-ray crystallography. In addition, evidence for electronic communication between the redox-active ferrocenecarboxylate ligands has been found in the trans-positioned product ***trans*-2c** ($\Delta E_{1/2}$ value of 100 mV), while the split in both cis-positioned products ***cis*-2a** and ***cis*-2b** is not similarly obvious. Furthermore, a second Mo_2-based oxidation of $[Mo_2]^{5+}/[Mo_2]^{6+}$ is evident in ***trans*-2c**, most likely due to the strong electron-donating effect of the aryl substituent -OMe. Finally, a plausible transformation mechanism is proposed based on the newly identified ligand basicity order.

All in all, the presented work provides insights into the controllable design of structural motifs, paving the way toward redox-active supramolecular structures. Since *trans*-$[Mo_2(DAniF)_2(NCCH_3)_4][BF_4]_2$[30] was already synthesized but has not been applied so far, a synthetic strategy to obtain multi redox-active ladder type oligomer is currently being established in our laboratories.

EXPERIMENTAL SECTION

General Procedure and Materials. All preparations and reactions were carried out under argon using standard Schlenk techniques. All solvents were dried using standard procedures.[55] *N*,*N*′-Diphenylformamidine (HDPhF) was purchased from Sigma-Aldrich and used as received. *N*,*N*′-di-*p*-(trifluoromethylphenyl)formamidine (HDTfmpF) and *N*,*N*′-di-*p*-anisylformamidine (HDAniF) were synthesized by following published procedures.[56] Precursor ***cis*-1** was prepared according to a literature procedure[3] and is in this paper referred to the formula $[Mo_2(O_2C\text{-}Fc)_2(NCCH_3)_4][BF_4]_2$ after overnight drying. NMR measurements were performed on a Bruker AVANCE-DPX-400 and Avance-DRX-400 MHz spectrometer (^{1}H: 400.13 MHz; ^{13}C: 100.62 MHz; ^{19}F: 376.5 MHz). Chemical shifts were reported in ppm and referenced to the solvent as internal standard. Elemental analyses were carried out at the microanalytical laboratory of Technische Universität München. UV−vis spectra were recorded with a Jasco V-550 spectrophotometer. Solution spectra were measured in a quartz cell with a 1 cm path length (background: solvent vs solvent), with a sample concentration of 30 μM. Cyclic and differential pulse voltammograms were recorded in three testing conditions (0.1 M of electrolyte solution), including T1: CH_2Cl_2 and $[n\text{-}Bu_4N][PF_6]$; T2: CH_2Cl_2 and $[n\text{-}Bu_4N][BF_4]$; and T3: CH_2Cl_2/CH_3CN (1/1) and $[n\text{-}Bu_4N][BF_4]$, on a Gamry Reference 600 voltammetric analyzer with a platinum working electrode (diameter = 1 mm), a Pt/Ti wire auxiliary electrode, and a Ag/AgCl reference electrode. The concentration of all the samples was 2.0 mM, and all the potential values were referenced to Fc/Fc^+.

Synthesis of *cis*-$[Mo_2(O_2C\text{-}Fc)_2(DPhF)_2]$ (***cis*-2a**). A solution of 2 equiv of *N*,*N*′-diphenylformamidine (78.5 mg, 400 μmol) and $NaOCH_3$ (21.6 mg, 400 μmol) in CH_3CN (10 mL) was stirred for 15 min and then added to a CH_3CN (10 mL) solution of 1 equiv of *cis*-$[Mo_2(O_2C\text{-}Fc)_2(NCCH_3)_4][BF_4]_2$ (***cis*-1**; 198 mg, 200 μmol). The reaction mixture was stirred for 5 h at room temperature to yield an orange solid and a dark brown solution. The solid was separated and dried under reduced pressure. The obtained orange solid was redissolved in 8 mL of CH_2Cl_2 and layered with *n*-pentane (8 mL) and diethyl ether (1.5 mL). A small amount of tiny crystals and precipitate both appeared, verified as cis and trans mixture by ^{1}H NMR spectroscopy. Therefore, a secondary crystallization is necessary to obtain the pure product, with the filtrate of the first crystallization dried and redissolved in 6 mL of CH_2Cl_2 and layered with *n*-pentane (6 mL) and diethyl ether (1 mL). Small bright orange, air- and moisture-sensitive crystals formed over a couple of nights. The orange crystals were collected, washed with *n*-pentane, and dried under vacuo. Compound ***cis*-2a** was obtained in a crystalline yield of 25%. ^{1}H NMR (CD_2Cl_2): δ 8.74 (s, 2H, NCHN), 7.13 (t, 8H, H_{ph}), 7.01 (t, 4H, H_{ph}), 6.77 (d, 8H, H_{ph}), 4.99 (t, 4H, H_{cp}), 4.40 (t, 4H, H_{cp}), 4.10 (s, 10H, H_{cp}). ^{13}C NMR (CD_2Cl_2): δ 180.6 (COO^-), 156.8 (NCHN), 149.7 (C_{ph-N}), 129.7 (C_{ph}), 124.4 (C_{ph}), 122.7 (C_{ph}), 74.54 ($C_{quat\text{-}cp}$), 71.66 (C_{cp}), 70.88 (C_{cp}), 70.73 (C_{cp}). Anal. Calcd for ($C_{48}H_{40}Fe_2Mo_2N_4O_4$) = $[Mo_2(O_2C\text{-}Fc)_2(DPhF)_2]$: C, 55.41; H, 3.88; N, 5.38. Found: C, 55.23; H, 3.80; N, 5.31.

Synthesis of *cis*-$[Mo_2(O_2C\text{-}Fc)_2(DTfmpF)_2]$ (***cis*-2b**) and *trans*-$[Mo_2(O_2C\text{-}Fc)_2(DAniF)_2]$ (***trans*-2c**). Compounds ***cis*-2b** and ***tran*-2c** were obtained with the same synthetic procedure as for ***cis*-2a** by using HDTfmpF and HDAniF instead of HDPhF, respectively. Bright orange, air- and moisture-sensitive crystals of ***cis*-2b** as well as ***trans*-2c** formed via two times crystallization, which were suitable for X-ray crystallographic measurements. The crystals were collected, washed with *n*-pentane, and dried under vacuo. Compounds ***cis*-2b** and ***trans*-2c** were obtained in crystalline yields of 20 and 25%, respectively.

Compound ***cis*-2b**: ^{1}H NMR (CD_2Cl_2): δ 8.74 (s, 2H, NCHN), 7.39 (d, 8H, H_{ph}, $^3J_{HH}$ = 8.0 Hz), 6.82 (d, 8H, H_{ph}, $^3J_{HH}$ = 8.0 Hz), 5.02 (t, 4H, H_{cp}), 4.45 (t, 4H, H_{cp}), 4.08 (s, 10H, H_{cp}). ^{13}C NMR (CD_2Cl_2): δ 181.9 (COO^-), 156.9 (NCHN), 152.1 (C_{ph-N}), 127.0 (q, C_{ph}, $^3J_{CF}$ = 3.70 Hz), 126.7 (q, C_{ph}, $^2J_{CF}$ = 32.4 Hz), 124.8 (q, C_{ph}, $^1J_{CF}$ = 270 Hz), 122.7 (s, C_{ph}), 73.83 ($C_{quat\text{-}cp}$), 72.11 (C_{cp}), 70.97 (C_{cp}), 70.75 (C_{cp}). ^{19}F NMR (CD_2Cl_2): δ −62.44 (s, CF_3). Anal. Calcd for ($C_{52}H_{36}F_{12}Fe_2Mo_2N_4O_4$) = $[Mo_2(O_2C\text{-}Fc)_2(DTfmpF)_2]$: C, 47.59; H, 2.76; N, 4.27. Found: C, 48.06; H, 2.99; N, 4.25.

Compound ***trans*-2c**: ^{1}H NMR (CD_2Cl_2): δ 8.60 (s, 2H, NCHN), 6.73 (d, 8H, H_{ph}, $^3J_{HH}$ = 8.8 Hz), 6.69 (d, 8H, H_{ph}, $^3J_{HH}$ = 8.8 Hz), 4.98 (t, 4H, H_{cp}), 4.39 (t, 4H, H_{cp}), 4.10 (s, 10H, H_{cp}), 3.73 (s, 12H, OCH_3). ^{13}C NMR (CD_2Cl_2): δ 180.1 (COO^-), 156.9 ($C_{ph-OCH3}$), 156.6 (NCHN), 143.1 (C_{ph-N}), 123.6 (C_{ph}), 114.8 (C_{ph}), 74.68 ($C_{quat\text{-}cp}$), 71.56 (C_{cp}), 70.82 (C_{cp}), 70.71 (C_{cp}), 55.94 (OCH_3). Anal. Calcd for ($C_{52}H_{48}Fe_2Mo_2N_4O_8$) = $[Mo_2(O_2C\text{-}Fc)_2(DAniF)_2]$: C, 53.82; H, 4.17; N, 4.83. Found: C, 53.68; H, 4.42; N, 4.85.

X-ray Structure Determination. Data were collected on a single-crystal X-ray diffractometer equipped with a CCD detector (Bruker APEX II, κ-CCD), a rotating anode (Bruker AXS, FR591) with Mo K_α radiation (λ = 0.71073 Å), a Montel mirror monochromator (**2a**−**2c**) by using the *APEX2* software package.[57] The measurements were performed on a single crystal coated with perfluorinated ether. The crystal was fixed on the top of a glass fiber and transferred to the diffractometer. The crystal was frozen under a stream of cold nitrogen. A matrix scan was used to determine the initial lattice parameters. Reflections were merged and corrected for Lorenz and polarization effects, scan speed, and background using *SAINT*.[58] Absorption corrections, including odd- and even-ordered spherical harmonics were performed using *SADABS*.[58] Space-group assignments were based on systematic absences, *E* statistics, and successful refinement of the structures. Structures were solved by direct methods as implemented in the *APEX2* software package[57] based on *SHELXS-97*[59] and were refined

DOI: 10.1021/acs.inorgchem.5b00964
Inorg. Chem. 2015, 54, 6631−6640

against all data using *SHELXLE*[60] in conjunction with *SHELXL-2014*.[61] Hydrogen atoms were assigned to ideal positions and refined using a riding model with an isotropic thermal parameter 1.2 times that of the attached carbon atom (1.5 times for methyl hydrogen atoms). If not mentioned otherwise, non-hydrogen atoms were refined with anisotropic displacement parameters. Full-matrix least-squares refinements were carried out by minimizing $\Sigma w(F_o^2 - F_c^2)^2$ with *SHELXL-97*[62] weighting scheme. Neutral atom scattering factors for all atoms and anomalous dispersion corrections for the non-hydrogen atoms were taken from *International Tables for Crystallography*.[63] Images of the crystal structures were generated by MERCURY.[64]

■ ASSOCIATED CONTENT

Supporting Information

XYZ coordinates, X-ray crystallographic data in CIF formats, and listings of spectroscopic and crystallographic details. The Supporting Information is available free of charge on the ACS Publications website at DOI: 10.1021/acs.inorgchem.5b00964. CCDC 1058944 (***cis*-2a**), CCDC 1058945 (***cis*-2b**), CCDC 1058946 (***trans*-2c**) contain the supplementary crystallographic data for this paper.

■ AUTHOR INFORMATION

Corresponding Author

*E-mail: fritz.kuehn@ch.tum.de.

Author Contributions

[§]Chair of Inorganic Chemistry, Department of Chemistry and CRC, TUM.

Notes

The authors declare no competing financial interest.

■ ACKNOWLEDGMENTS

Support from the China Scholarship Council (stipend to X.-M.C.) and the Stiftung Stipendienfonds des Fonds der Chemischen Industrie (stipend to T.K.Z.) and the TUM Graduate School is gratefully acknowledged.

■ REFERENCES

(1) Cotton, F. A.; Curtis, N. F.; Harris, C. B.; Johnson, B. F. G.; Lippard, S. J.; Mague, J. T.; Robinson, W. R.; Wood, J. S. *Science* **1964**, *145*, 1305−1307.

(2) Cotton, F. A.; Murillo, C. A.; Walton, R. A. *Multiple Bonds Between Metal Atoms*, 3rd ed.; Springer Science and Business Media Inc.: New York, 2005; pp 69−182.

(3) Cai, X.-M.; Höhne, D.; Köberl, M.; Cokoja, M.; Pöthig, A.; Herdtweck, E.; Haslinger, S.; Herrmann, W. A.; Kühn, F. E. *Organometallics* **2013**, *32*, 6004−6011.

(4) Höhne, D.; Herdtweck, E.; Pöthig, A.; Kühn, F. E. *Dalton Trans.* **2014**, *43*, 15367−15374.

(5) Köberl, M.; Cokoja, M.; Herrmann, W. A.; Kühn, F. E. *Dalton Trans.* **2011**, *40*, 6834−6859.

(6) Köberl, M.; Cokoja, M.; Bechlars, B.; Herdtweck, E.; Kühn, F. E. *Dalton Trans.* **2011**, *40*, 11490−11496.

(7) Fritsch, N.; Wick, C. R.; Waidmann, T.; Dral, P. O.; Tucher, J.; Heinemann, F. W.; Shubina, T. E.; Clark, T.; Burzlaff, N. *Inorg. Chem.* **2014**, *53*, 12305−12314.

(8) Chisholm, M. H.; Patmore, N. J.; Reed, C. R.; Singh, N. *Inorg. Chem.* **2010**, *49*, 7116−7122.

(9) Xue, W.-M.; Kühn, F. E.; Herdtweck, E.; Li, Q. *Eur. J. Inorg. Chem.* **2001**, 213−221.

(10) Xue, W.-M.; Kühn, F. E. *Eur. J. Inorg. Chem.* **2001**, 2041−2047.

(11) Brown-Xu, S. E.; Chisholm, M. H.; Durr, C. B.; Gustafson, T. L.; Naseri, V.; Spilker, T. F. *J. Am. Chem. Soc.* **2012**, *134*, 20820−20826.

(12) Wilkinson, L. A.; McNeill, L.; Patmore, N. J. *J. Am. Chem. Soc.* **2013**, *135*, 1723−1726.

(13) Wilkinson, L. A.; McNeil, L.; Scattergood, P. A.; Patmore, N. J. *Inorg. Chem.* **2013**, *52*, 9683−9691.

(14) Brown-Xu, S. E.; Chisholm, M. H.; Durr, C. B.; Lewis, S. A.; Spilker, T. F.; Young, P. J. *Chem. Sci.* **2014**, *5*, 2657−2666.

(15) Cai, X.-M.; Riener, K.; Herdtweck, E.; Pöthig, A.; Kühn, F. E. *Inorg. Chem.* **2015**, *54*, 3272−3280.

(16) Xiao, X.; Liu, C.-Y.; He, Q.; Lu, X. *Inorg. Chem.* **2013**, *52*, 12624−12633.

(17) Cotton, F. A.; Murillo, C. A.; Zhao, Q. *Inorg. Chem.* **2009**, *48*, 11755−11766.

(18) Cotton, F. A.; Li, Z.; Murillo, C. A. *Inorg. Chem.* **2009**, *48*, 11847−11852.

(19) Cotton, F. A.; Lin, C.; Murillo, C. A. *Acc. Chem. Res.* **2001**, *34*, 759−771.

(20) Han, M. J.; Liu, C. Y.; Tian, P. F. *Inorg. Chem.* **2009**, *48*, 6347−6349.

(21) Tan, Z. F.; Liu, C. Y.; Li, Z.; Meng, M.; Weng, N. S. *Inorg. Chem.* **2012**, *51*, 2212−2221.

(22) Han, L. J.; Fan, L. Y.; Meng, M.; Wang, X.; Liu, C. Y. *Dalton Trans.* **2011**, *40*, 12832−12838.

(23) Shu, Y.; Lei, H.; Tan, Y. N.; Meng, M.; Zhang, X. C.; Liu, C. Y. *Dalton Trans.* **2014**, *43*, 14756−14765.

(24) Cotton, F. A.; Lin, C.; Murillo, C. A. *Inorg. Chem.* **2001**, *40*, 472−477.

(25) Cotton, F. A.; Lin, C.; Murillo, C. A. *Inorg. Chem.* **2001**, *40*, 575−577.

(26) Cotton, F. A.; Daniels, L. M.; Lin, C.; Murillo, C. A. *J. Am. Chem. Soc.* **1999**, *121*, 4538−4539.

(27) Cotton, F. A.; Lin, C.; Murillo, C. A. *Inorg. Chem.* **2001**, *40*, 478−484.

(28) Brown, D. J.; Chisholm, M. H.; Gallucci, J. C. *Dalton Trans.* **2008**, 1615−1624.

(29) Cayton, R. H.; Chisholm, M. H.; Huffman, J. C.; Lobkovsky, E. B. *J. Am. Chem. Soc.* **1991**, *113*, 8709−8724.

(30) Cotton, F. A.; Lin, C.; Murillo, C. A. *Inorg. Chem.* **2004**, *43*, 2267−2276.

(31) Cotton, F. A.; Kühn, F. E.; Yokochi, A. *Inorg. Chim. Acta* **1996**, *252*, 251−256.

(32) Cotton, F. A.; Kühn, F. E. *Inorg. Chim. Acta* **1996**, *252*, 257−264.

(33) Chisholm, M. H.; Cotton, F. A.; Daniels, L. M.; Folting, K.; Huffman, J. C.; Iyer, S. S.; Lin, C.; Macintosh, A. M.; Murillo, C. A. *J. Chem. Soc., Dalton Trans.* **1999**, 1387−1392.

(34) Majumdar, M.; Patra, S. K.; Kannan, M.; Dunbar, K. R.; Bera, J. K. *Inorg. Chem.* **2008**, *47*, 2212−2222.

(35) Bunting, P.; Chisholm, M. H.; Gallucci, J. C.; Lear, B. J. *J. Am. Chem. Soc.* **2011**, *133*, 5873−5881.

(36) Brown-Xu, S. E.; Chisholm, M. H.; Durr, C. B.; Spilker, T. F.; Young, P. J. *Chem. Sci.* **2015**, *6*, 1780−1791.

(37) Chisholm, M. H.; Durr, C. B.; Gustafson, T. L.; Kender, W. T.; Spilker, T. F.; Young, P. J. *J. Am. Chem. Soc.* **2015**, *137*, 5155−5162.

(38) Cotton, F. A.; Feng, X.; Matusz, M. *Inorg. Chem.* **1989**, *28*, 594−601.

(39) Lin, C.; Protasiewicz, J. D.; Smith, E. T.; Ren, T. *Inorg. Chem.* **1996**, *35*, 6422−6428.

(40) Cotton, F. A.; Daniels, L. M.; Wikinson, C. C. *J. Am. Chem. Soc.* **2002**, *124*, 9249−9256.

(41) Cotton, F. A.; Daniels, L. M.; Hillard, E. A.; Murillo, C. A. *Inorg. Chem.* **2002**, *41*, 1639−1644.

(42) Cotton, F. A.; Pedersen, E. *Inorg. Chem.* **1975**, *14*, 399−400.

(43) Murillo, C. A. *Inorg. Chim. Acta* **2015**, *424*, 3−13.

(44) Chisholm, M. H.; Brown-Xu, S. E.; Spilker, T. F. *Acc. Chem. Res.* **2015**, *48*, 877−885.

(45) Falvello, L. R.; Foxman, B. M.; Murillo, C. A. *Inorg. Chem.* **2014**, *53*, 9441−9456.

(46) Chisholm, M. H. *Coord. Chem. Rev.* **2015**, *282*−*283*, 60−65.

(47) Boyd, D. A.; Crutchley, R. J.; Fanwick, P. E.; Ren, T. *Inorg. Chem.* **2010**, *49*, 1322−1324.

(48) Boyd, D. A.; Cao, Z.; Song, Y.; Wang, T.-W.; Fanwick, P. E.; Crutchley, R. J.; Ren, T. *Inorg. Chem.* **2010**, *49*, 11525−11531.

DOI: 10.1021/acs.inorgchem.5b00964
Inorg. Chem. 2015, 54, 6631−6640

(49) Cotton, F. A.; Donahue, J. P.; Murillo, C. A. *J. Am. Chem. Soc.* **2003**, *125*, 5436−5450.
(50) Cotton, F. A.; Donahue, J. P.; Lin, C.; Murillo, C. A. *Inorg. Chem.* **2001**, *40*, 1234−1244.
(51) Cotton, F. A.; Lin, C.; Murillo, C. A. *J. Am. Chem. Soc.* **2001**, *123*, 2670−2671.
(52) Cotton, F. A.; Murillo, C. A.; Wang, X.; Wilkinson, C. C. *Dalton Trans.* **2006**, 4623−4631.
(53) Richardson, D. E.; Taube, H. *Inorg. Chem.* **1981**, *20*, 1278−1285.
(54) Chisholm, M. H.; Patmore, N. J. *Acc. Chem. Res.* **2007**, *40*, 19−27.
(55) Armarego, W. L. F.; Chai, C. *Purification of Laboratory Chemicals*; Elsevier Science: Amsterdam, 2009; pp 25−30.
(56) Binobaid, A.; Iglesias, M.; Beetstra, D. J.; Kariuki, B.; Dervisi, A.; Fallis, I. A.; Cavell, K. J. *Dalton Trans.* **2009**, 7099−7112.
(57) *APEX Suite of Crystallographic Software, APEX 2*, Version 2008.4; Bruker AXS Inc.: Madison, USA, 2008.
(58) *SAINT, version 7.56a, SADABS, version 2008.1*; Bruker AXS Inc.; Madison, USA, 2008.
(59) Sheldrick, G. M. *SHELXL-97*, University of Göttingen: Göttingen, Germany, 1998.
(60) Huebschle, C. B.; Sheldrick, G. M.; Dittrich, B. *SHELXLE, J. Appl. Crystallogr.* **2011**, *44*, 1281−1284.
(61) Sheldrick, G. M. *SHELXL-2014*, University of Göttingen: Göttingen, Germany, 2014
(62) Sheldrick, G. M. *SHELXL-97*, University of Göttingen: Göttingen, Germany, 1998.
(63) Wilson, A. J. C. *International Tables for Crystallography*; Kluwer Academic Publishers: Dordrecht, The Netherlands, 1992.
(64) Macrae, C. F.; Bruno, I. J.; Chisholm, J. A.; Edgington, P. R.; McCabe, P.; Pidcock, E.; Rodriguez-Monge, L.; Taylor, R.; Streek, J. van de; Wood, P. A. *J. Appl. Cryst.* **2008**, *41*, 466−470.

DOI: 10.1021/acs.inorgchem.5b00964
Inorg. Chem. 2015, 54, 6631−6640